REVISION 1

Gungerite, $TlAs_5Sb_4S_{13}$, a new thallium sulfosalt with a complex structure containing covalent As–As bonds

ANATOLY V. KASATKIN[1], JAKUB PLÁŠIL[2§], EMIL MAKOVICKY[3], NIKITA V. CHUKANOV[4], RADEK ŠKODA[5], ATALI A. AGAKHANOV[1] AND MIKHAIL V. TSYGANKO[6]

[1] Fersman Mineralogical Museum of the Russian Academy of Sciences, Leninsky Prospekt 18-2, 119071 Moscow, Russia

[2] Institute of Physics ASCR, v.v.i., Na Slovance 1999/2, 18221 Prague 8, Czech Republic

[3] Department of Geoscience and Resource Management, University of Copenhagen, Østervoldgade 10, DK-1350, Copenhagen K, Denmark

[4] Institute of Problems of Chemical Physics, Russian Academy of Sciences, Chernogolovka, 142432, Moscow Region, Russia

[5] Department of Geological Sciences, Faculty of Science, Masaryk University, Kotlářská 2, 611 37, Brno, Czech Republic

[6] 40 Let Oktyabrya street 15, Kalya, Severouralsk, Sverdlovskaya Oblast', 624474 Russia

ABSTRACT

Gungerite, $TlAs_5Sb_4S_{13}$, is a new mineral from the Vorontsovskoye gold deposit in Northern Urals. It occurs in limestone breccias composed of calcite and dolomite, and cemented by orpiment, pyrite, realgar, stibnite, and minor baryte and quartz. It belongs to the latest phases among sulfosalts (chiefly Tl–As–Sb ones) present in the ore. The empirical formula (based on the sum of all atoms = 23 *pfu*) is $Tl_{0.99}As_{5.29}Sb_{3.77}S_{12.95}$. The Raman spectrum exhibits bands corresponding to As–S and Sb–S stretching vibrations, and a band at 263 cm^{-1} which is

§ Email: plasil@fzu.cz

assigned to As–As stretching vibrations. Gungerite is bright orange with an orange streak, greasy luster and perfect cleavage on {010}. It is translucent in thin fragments. The calculated density is 4.173 g/cm^3. In reflected light, the mineral is yellowish-white with very weak bireflectance. In crossed polars it is distinctly anisotropic but anisotropy effects are masked by strong internal reflections of bright orange color. Gungerite is orthorhombic, with the space group *Pbcn*. Unit-cell parameters determined from the single-crystal X-ray diffraction data are as follows: a = 20.1958(3) Å, b = 11.5258(2) Å, c = 20.1430(2) Å, V = 4688.74(12) Å^3 (Z = 8). The crystal structure consists of doughnut-shaped (As,Sb)–S clusters, which have van der Waals contacts to most of the surroundings, and are connected to them only by sparse cation–sulfur bonds. These clusters are formed by a chelating mirror-symmetrical group which is 'stacked' on, around, and along rods of the TlS_9 coordination polyhedra; these rods are oriented parallel to [010]. An individual doughnut-shaped cluster with a central TlS_9 polyhedron half-inserted into it contains one As–As bond 2.449 Å long. The polar Tl rods form a chess-board arrangement with occasional stacking errors leading to twinning on (101). The large and complex structure of gungerite shows remote similarities to that of gillulyite and the rod-like structure of lorándite.

Keywords: gungerite; new mineral species; Tl–As–Sb sulfosalt; Raman spectroscopy; crystal structure; covalent bonds; Vorontsovskoe gold deposit.

INTRODUCTION

Thallium and its compounds play a very important role in a wide variety of industrial applications (Gresham and Lawrey 2018; https://www.usgs.gov/centers/nmic/thallium-statistics-and-information): they are applied in the manufacture of electronic devices, optical lenses with a high refractive index, semiconductor materials, alloys, gamma radiation

detection equipment, infrared radiation detection and transmission equipment, crystalline filters for light diffraction for acoustic-optical measuring devices, low-temperature thermometers, in the synthesis of organic compounds, and in a high-density liquid for sink-float separation of minerals. Also, research activity with thallium is ongoing to develop high-temperature superconducting materials for such applications as magnetic resonance imaging, storage of magnetic energy, magnetic propulsion, and electric power generation and transmission. Trace amounts of thallium are used as a contrast agent in the visualization of cardiac function and tumors. On the other hand, thallium compounds show a very strong level of toxicity and should be strictly controlled to prevent harm to humans and the environment. Although thallium is moderately abundant in the Earth's crust [for instance, the average content of Tl in granites is 1.5 ppm (Turekian and Wedepohl 1961)], it is mostly dissipated in associated potassium minerals in clays, granites, and soils, and is not generally considered to be commercially recoverable from those materials. The major sources of recoverable thallium are gold and complex sulfide ores ores (Ikramuddin, 1985; Karbowska, 2016). Because of the above, much attention of geologists and mineralogists is given to the research of gold deposits that bear Tl-mineralization and to the study of new Tl-bearing mineral species and their structures.

Herein, we describe the new sulfosalt mineral gungerite containing thallium as a species-defining element. Gungerite was found at the Vorontsovskoe gold deposit located in Northern Urals, Russia. This deposit is unique with regard to the diversity and originality of its Tl-Hg-Mn-As-Sb-S mineralization while gungerite is a remarkable example of a sulfosalt having complicated complex crystal structure both with covalent and van der Waals bonds. Its name honors Yuri Vladimirovich Gunger (born August 6th, 1961), a mining engineer and surveyor, famous historian and expert of Northern Urals. Both the name and the new mineral were approved by the Commission on New Minerals, Nomenclature and Classification of the

International Mineralogical Association (the proposal IMA2020-009). The holotype specimen is deposited in the collections of the Fersman Mineralogical Museum of the Russian Academy of Sciences, Moscow, Russia, with registration number 5518/1.

OCCURRENCE

Specimens containing the new mineral were collected in March 2016 at the main ore stockpile of the Vorontsovskoe gold deposit, approximately 13 km to the south of the city of Krasnotur'insk, Sverdlovskaya Oblast', Northern Urals, Russia (59° 38' 50" N, 60° 12' 52" E). A detailed description of the deposit, its genesis, geology and composition of main types of ores can be found elsewhere (Sazonov et al. 1998; Vikentyev et al. 2016; Murzin et al. 2017; Kasatkin et al. 2018a, b, 2019, 2020a). Kasatkin et al. (2020c) recently summarized the history of the study of the deposit and its geological background, provided the description of main mineral assemblages and compiled an exhaustive list of 209 mineral species identified there. Among them, eight are new minerals discovered by our team and all of them are sulfosalts: vorontsovite, ferrovorontsovite (Kasatkin et al. 2018a), tsygankoite (Kasatkin et al. 2018b), gladkovskyite (Kasatkin et al. 2019), luboržákite (Kasatkin et al. 2020a), pokhodyashinite (Kasatkin et al. 2020b), auerbakhite (Kasatkin et al. 2021) and gungerite described herein.

Gungerite was found in carbonate breccias composed mainly of calcite and dolomite and cemented by orpiment, pyrite, realgar, stibnite and minor baryte and quartz. Other associated minerals include bernardite, minerals of chabournéite–dalnegroite and vorontsovite–ferrovorontsovite series, cinnabar, coloradoite, gold, greigite, hutchinsonite, parapierrotite and routhierite. Most likely, gungerite was formed in the latest stage of the low-temperature hydrothermal process.

PHYSICAL PROPERTIES

Among all the new minerals discovered at the Vorontsovskoe deposit, gungerite is the only one that forms macroscopic segregations visible by the naked eye: its fine-grained aggregates fill areas up to 0.5 × 0.2 cm on the surface of carbonate breccias (Figs. 1 and 2). It has a bright orange color, orange streak and greasy luster. Gungerite is translucent in thin fragments, brittle and has an uneven fracture. Perfect cleavage on {010} has been observed. The new mineral does not exhibit any fluorescence under UV radiation. The Vickers hardness (VHN, 10 g load) is 84 kg/mm^2 (range 74–98 kg/mm^2, n = 4) corresponding to a Mohs hardness of 2–2½. The density of gungerite could not be measured because of the absence of suitable heavy liquids. The density calculated based on the empirical formula (Z = 8) and the unit-cell volume determined from the single-crystal X-ray diffraction data is 4.173 g/cm^3. In reflected light, gungerite is yellowish-white, but at contact with stibnite it looks light gray with a weak bluish tint. Bireflectance is very weak. The new mineral is distinctly anisotropic but anisotropy effects are masked by internal reflections of bright orange color. The latter is seen even in one nicol, while in crossed polars in air and especially in immersion they are extremely abundant and strong. Quantitative reflectance measurements were performed in the air relative to a WTiC standard using a Universal Microspectrophotometer UMSP 50 (Opton-Zeiss, Germany). Reflectance values are given in Table 1.

RAMAN SPECTROSCOPY

The Raman spectrum of gungerite (Fig. 3) was obtained from the polished section utilizing a Horiba Labram HR Evolution spectrometer. This dispersive, edge-filter-based system is equipped with an Olympus BX 41 optical microscope, a diffraction grating with 600 grooves per millimeter, and a Peltier-cooled, Si-based charge-coupled device (CCD) detector. After careful tests with different lasers (473, 532 and 633 nm), the 633 nm He-Ne laser with

126 the beam power of 1 mW at the sample surface was selected for spectra acquisition to
127 minimize analytical artifacts. Raman signal was collected in the range of 600–50 cm^{-1} with a
128 50x objective and the system operated in the confocal mode; beam diameter was ~2.6 μm and
129 the lateral resolution ~5 μm. Wavenumber calibration was done using the Rayleigh line and
130 low-pressure Ne-discharge lamp emissions. The wavenumber accuracy was ~0.5 cm^{-1}, and
131 the spectral resolution was ~2 cm^{-1}. Band fitting was done after appropriate background
132 correction, assuming combined Lorentzian–Gaussian band shapes using Voigt function
133 (PeakFit; Jandel Scientific Software).

134 Preliminary assignment of the Raman bands was made by analogy with simple
135 sulfides. Raman bands of As–S stretching vibrations in the Raman spectra of orpiment, As_2S_3,
136 and realgar, AsS, are observed in the range of 360–290 cm^{-1} (Forneris 1969; Minceva-
137 Sukarova et al. 2003). In these minerals, the As–S distances are in the range of 2.21–2.31 Å
138 (Morimoto 1954; Mullen and Nowacki 1972). The largest distances correspond to the lowest
139 frequencies of As–S stretching vibrations. In gungerite, the As–S distances vary from 2.206 to
140 2.320 Å. Consequently, bands of As–S stretching vibrations are expected to be in the range of
141 370–280 cm^{-1}.

142 The band of the highest intensity adhering to Sb–S stretching vibrations in the Raman
143 spectrum of stibnite has been observed within the range of 308–280 cm^{-1} (Mernagh and
144 Trudu 1993; Minceva-Sukarova et al. 2003; Kharbish et al. 2009; Makreski et al. 2014). This
145 is corresponding to the band located at 294 cm^{-1} in gungerite. An additional band observed in
146 the Raman spectra of stibnite (in the range 251–236 cm^{-1}) conforms to the shoulder at 240
147 cm^{-1} in the spectrum of gungerite. This band was assigned to the bending mode of the SbS_3
148 units (Frost et al. 2010).

149 A more precise assignment of Raman bands of gungerite can be made based on the
150 comparison with Raman spectra of thallium sulfosalts. In the IR spectrum of lorándite,

$TlAsS_2$, bands of As–S stretching vibrations are observed in the range of 380–350 cm^{-1}. The comparison of the Raman spectra of lorándite with the Raman spectra of Sb-bearing thallium sulfosalts containing pyramidal $(As,Sb)S_3$ units (parapierrotite, rebulite, and vrbaite) resulted in the following assignment of Raman bands of SbS_3 units (Makreski et al. 2014; Kharbish 2011): 302–310 cm^{-1} to the asymmetric stretching mode of SbS_3; 334 cm^{-1} to the symmetric stretching mode of SbS_3; 282 and 270 cm^{-1} (weak bands) to the symmetric and asymmetric bending modes of SbS_3, respectively. Consequently, the bands of gungerite observed in the range 400–340 cm^{-1} should be assigned to As–S stretching vibrations and the bands in the range 340–280 cm^{-1} are due to both As–S and Sb–S stretching vibrations. Noteworthy is that no strong Raman bands are observed in the range 265–250 cm^{-1} of all above-mentioned sulfides and sulfosalts except gungerite.

Based on the estimated As–As bond force constant value of 1.09 mdyn/Å, Muniz-Miranda et al. (1996) assigned the bands at 173 and 184 cm^{-1} in the Raman spectrum of realgar to modes with a significant contribution of As–As stretching. The As–As bond length in realgar is equal to 2.57 Å. For gungerite having a shorter As–As bond (2.4487 Å long), a higher frequency of As–As stretching vibrations should be expected.

Unlike other Sb-bearing thallium sulfosalts containing pyramidal $(As,Sb)S_3$ units, gungerite is characterized by the presence of a short As–As bond in the crystal structure and the presence of the strong band at 263 cm^{-1} in the Raman spectrum. Based on this fact, the band at 263 cm^{-1} was assigned to As–As stretching vibrations. This assignment is in a good agreement with the Raman spectrum of arsenolamprite (Thomas and Davidson 2010), the strongest Raman band of which is observed at 253 cm^{-1}.

It is to be noted that the As–As bond length in sulfosalts varies in wide ranges. For example, in wakabayashilite these bands are about 2.84 Å long. Correspondingly, no bands in the range of 230 – 300 cm^{-1} are observed in the Raman spectrum of wakabayashilite (Bindi et

al 2014). A band at 268 cm^{-1} was observed in the Raman spectrum of realgar by Cheng et al. (2017), but the assignment of this band is ambiguous. Moreover, this band was not detected in Raman spectra of realgar in other works. Most probably, the band at 268 cm^{-1} corresponds to pararealgar formed from realgar under laser beam (Muniz-Miranda et al. 1996).

The assignment of Raman bands with wavenumbers below 200 cm^{-1} is ambiguous. Presumably, these bands correspond to soft mixed lattice modes involving As–S–As bending and Tl–S stretching vibrations.

CHEMICAL ANALYSIS

Quantitative chemical analyses were carried out using a Cameca SX-100 electron microprobe operated in wavelength-dispersion spectroscopy (WDS) mode applying an accelerating voltage of 25 kV, a beam current of 10 nA and a beam diameter of 1 μm. Analytical data (for 19 points) and used standards are given in Table 2. Contents of other elements with atomic numbers larger than that of carbon were found to be below detection limits. The empirical formula (based on the sum of all atoms = 23 *pfu*) is: $Tl_{0.99}As_{5.29}Sb_{3.77}S_{12.95}$. The ideal chemical formula is $TlAs_5Sb_4S_{13}$, requiring Tl 13.78, As 25.26, Sb 32.85, S 28.11, total 100 wt. %.

X-RAY CRYSTALLOGRAPHY AND STRUCTURE DETERMINATION

Powder X-ray diffraction

Powder X-Ray diffraction data (Table 3) were obtained in Bragg-Brentano geometry using a PANalytical Empyrean powder diffractometer equipped with a Cu X-ray tube and PIXcel3D solid-state detector. A grain of gungerite about 1 mm^3 was placed onto a flat silicon wafer and mildly ground in acetone. The powder X-ray data were collected in the 2θ range 4–80° with a step of 0.013°, and an integrated counting time of 200 s per step (accumulation of

40 scans = total data-collection time was *ca*. 3 days). The unit-cell parameters were refined using the program Celref (Laugier and Bochu 2003). Theoretical *d*-spacings and intensities were calculated from the structure model using the PowderCell program (Kraus and Nolze 1996). The data obtained are affected by an extremely strong preferred orientation effect due to the perfect cleavage of gungerite on (010). Refined orthorhombic unit-cell parameters, obtained from the powder data, are: a = 20.18(1) Å, b = 11.528(3) Å, c = 20.14(1) Å, V = 4686(4) Å^3 (Z = 8).

Single-crystal X-ray diffraction

For the single-crystal diffraction experiment, a plate-like single-crystal fragment of gungerite, extracted from the polished section which had been analyzed using an electron microprobe, was selected under a polarized light microscope and mounted on a glass fiber. The diffraction experiment (see Table 4 for details) was performed at room temperature with a Rigaku SuperNova single-crystal diffractometer equipped with the Atlas S2 CCD detector and a microfocus MoK_α source. Data reduction was performed using CrysAlisPro Version 1.171.39.46 (Rigaku 2019). The data were corrected for Lorentz factor, polarization effect and absorption (multi-scan, ABSPACK scaling algorithm; Rigaku 2019). According to the single-crystal X-ray data, gungerite is orthorhombic, with the space group *Pbcn*. The unit-cell parameters determined from the single-crystal data are as follows: a = 20.1958(3) Å, b = 11.5258(2) Å, c = 20.1430(2) Å, V = 4688.74(12) Å^3 (Z = 8). The apparent pseudotetragonality of the [010] direction (Fig. 4a, b) expresses the large-scale geometry of the structure but is not supported by structure details. In this respect the structure reminds one of the structure of lorándite $TlAsS_2$ (Balić-Žunić et al. 1995) in which, however, distortions away from pseudotetragonality are more pronounced.

The crystal structure of gungerite was solved from the single-crystal X-ray data using intrinsic-phasing with the SHELXT program (Sheldrick 2015) and refined by the software Jana2006 (Petříček et al. 2014). The structure is strongly pseudo-tetragonal and during the import, into Jana2006 the twinning due to the metric merohedry (diffraction type I; Petříček et al. 2016) has been introduced as it is possible within the space-group test in Jana2006. Subsequent refinement returned reasonable fractions of the twin domains and resulted in excellent final *R*-values (Table 4). Anisotropic displacement parameters were refined for all atoms. Except for the higher average displacement parameter of Tl which is in agreement with its low charge and large interatomic Tl–S distances, and with the special way in which Tl is inserted in the structure (specified below), this structure is distinguished by fairly uniform and evenly distributed atomic displacement values for all atoms. The atom coordinates, atomic displacement parameters and site occupancies are given in Table 5 and selected interatomic distances in Table 6.

DESCRIPTION OF THE STRUCTURE

The crystal structure of gungerite is undoubtedly the most complex among all new sulfosalts discovered at the deposit. It contains 23 atomic sites, one site occupied purely by Tl, one site purely by Sb, three sites purely by As, and three Sb-dominant sites and two As-dominant sites that are mixed-occupied. The sites with mixed occupancies are as follows: Sb2 [0.840(12)Sb/0.160(12)As], Sb3 [0.844(13)Sb/0.156(13)As], Sb4 [0.781(11)Sb/0.219(11)As], As1 [0.820(12)As/0.180(12)Sb], and As2 [0.938(12)As/0.062(12)]. The crystal structure consists of (As,Sb)–S clusters, which have van der Waals contacts to most of the surroundings, and otherwise are connected to them only by sparse metal cation–sulfur bonds. These clusters have a peculiar arrangement, being ‘stacked’ on, around, and along Tl–S rods parallel to [010]. An individual cluster, always doughnut-shaped (or toroid-shaped) has a central Tl polyhedron half-inserted into it. The cluster is formed by a chelating mirror-

symmetrical group (‘*almost a molecule*’) which has Sb–As ‘*defect coordination cubes*’ as forceps (with some atoms missing from a perfect cube-model). Its two mirror-related arms are connected by the coordination pyramid of As3 (Fig. 5). One arm of the chelating group has an eyelet of doubly interconnected Sb1 and Sb3 as its terminal portion. Through the coordination pyramid of As1, the eyelet is connected to the centrally positioned pyramid of As3, from which starts the other arm of the chelating group. In the order of appearance, this arm consists of the coordination pyramid of As2, and a terminal eyelet of Sb2 and Sb4. These two Sb atoms are doubly interconnected *via* two sulfurs. A radially oriented ‘*tail-group*’ points out of the cluster and is formed by a covalent As–As bond (2.448 Å long), which connects As3 with As4. After the As4 polyhedron (which still is in a mirror-symmetric position with the rest of the ‘molecule’) As5 follows, which points sideways, counter to the *m* symmetry of the group. However, an As5 polyhedron from an adjacent ‘molecule’ is a mirror-symmetrical ‘plug’ that closes the doughnut body from the side which was left open by the original group (Fig. 5).

The coordination polyhedron of Tl is inserted in the cavity of the doughnut, and shares S atoms with the As/Sb coordination polyhedra (Figs. 5–7). The coordination number of Tl is nine. Among the bonds formed by Tl, six have lengths below 3.5 Å and three more are shorter than 3.6 Å. When all distances below 4.2 Å are included, the total is eleven Tl–S distances. Most remarkable are two short distances, 3.150 Å to S4 and 3.190 Å to S5, and a short Tl1–As3 bond having the length of 3.403 Å, well within the range of Tl–S distances (Table 6). The polyhedron shape is irregular, with three tetragon-shaped faces approximating a part of a distorted cube (Fig. 6). Thallium is embedded in one (010) face of the doughnut cluster, whereas S9 and S11 are a part of the surface opposite to it. Their 90°-rotated opposites, S9 and S11, are already a part of the adjacent cluster (Fig. 6). The sulfur sites S2, S3, S4, S5, and S8 surround Tl in the Tl-centered cluster. The faces of the Tl-centered polyhedron are as follows: broken tetragons S4–S8–S9–S11, S2–S5–S9–S11, and S3–S4–S9–S5; irregularly

broken pentagons S3–S4–S11–S9–S5 and S2–S9–S11–S8–S11; conspicuous triangles S2–S5–S9 and S4–S8–S11.

The As3 atom close to Tl, acts as a cap of the broad pentagon S2–S9–S11–S8–S11, which encircles a sulfur-free side of the Tl coordination polyhedron. It can represent the interaction of the lone electron pairs of Tl and As, opposed to the short bonds from As to S4, 5, and 9. The short Tl–As distance is analogous to those found in gabrielite, $Tl_2AgCu_2As_3S_7$ (3.11 Å), erniggliite, $Tl_2SnAs_2S_6$ (3.259 Å), richardsollyite, $TlPbAsS_3$ (3.397 Å), arsiccioite, $AgHg_2TlAs_2S_6$ (from 3.397 Å), and in several Tl sulfosalts with distances about and above 3.48 Å (summarized by Makovicky 2018). Thus, gungerite is one more example of cation–cation interactions, again with demonstrable involvement of lone electron pairs of both cations. Coordination polyhedra of thallium are interconnected and form 'rods' *via* sharing the S9–S11 joins (Fig. 6). These joins alternate their orientation by about 90° along the 'rod' of Tl-centered polyhedra which runs parallel to [010]. Although they necessarily are 'soft', these rods and the As–Sb clusters centered on them represent the substance of the gungerite structure (Figs. 6, 7).

The short covalent As3–As4 bond, which is 2.448 Å long (Figs. 5, 8), is analogous to such bonds in the small molecules, which are present in the structures of realgar, AsS (2.57 Å), alacranite, As_8S_9 (2.62 Å), pararealgar, As_4S_4 (2.48 and 2.53 Å), dimorphite, As_4S_3 (2.44 Å), and uzonite, As_4S_5 (2.55 Å) (summarized by Makovicky 2006). Except for uzonite, these molecules have two covalent As–As bonds each; only in the structure of realgar these bonds are distributed over different pairs of As atoms, whereas they are restricted to one As atom in the rest.

The coordination polyhedron of As3 is a pentagonal pyramid with two short bonds and three long distances in the base; the vertex is occupied by the arsenic atom As4. Besides two short As–S bonds (2.249 Å), As4 has two shorter weak bonds, 3.199 Å to S10 and 3.226 Å to

S13 (which, remarkably, also coordinate the As3 atom); the remaining As–S distances are longer than 4.17 Å. The shortest As–As contacts are 3.392 Å and 3.411 Å to As5, and 3.504 Å to directly opposing As4 in the As4–As5–As4–As5 ring. The Sb3 atom has a pentagonal coordination, with short bonds to S1 and S9, and three long distances to S8, S6, and S3. The As2 atom has a broad trapezoidal coordination, being bonded to S10 and S11, and has long distances to S5 and S12. The pentagonal coordination of As5 is based on short bonds to S6 and S7, long distances to S4 and S5, and this trapezoidal arrangement is completed by a long contact to Tl1 (4.141 Å). We can see that the activity of the lone electron pairs of arsenic is much less constrained in gungerite than, e.g., in orpiment.

The complex structure of gungerite makes a distinct imprint on the distribution of bonding and non-bonding distances. When we concentrate on the interdependence and counter-play of short strong As/Sb bonds and of the long distances generally opposing them, these pairs of distances concentrate around the values of 2.45 Å *vs*. 3.40 Å for the mixed Sb/As sites (where Sb prevails), whereas around 2.25–2.30 Å *vs*. 3.40 Å for the (mostly mixed) As/Sb sites (where As prevails). The As3–As4 pair of covalently bonded arsenic atoms (As–As 2.449 Å) has opposing distances at or above 3.8 Å. The As5 site has all the long distances at and above 3.65 Å, and one distant ligand (out of three) actually is missing.

Concerning the [010] stacking of clusters ('molecules') on an individual Tl rod, the consecutive clusters are related by the (100) *b*-glide, i.e. the orientation of As–As bond in them alternates, comprising ~90^{o} to one another in the (010) projection. In the stacking along the rod, the Sb-based group of the chelate always separates two consecutive As3–As4 groups, which have the same orientation in a stack of clusters around the Tl rod. For adjacent columns (Tl rods) which are arrayed along the *a*-axis, these configurations are related by inversion and they 'face' the opposite [00±1] directions (Fig. 9).

Interconnection of clusters and rods

Those clusters, which are attached to one thallium rod, face one another by their lone electron pairs and are connected *only* by one medium-strong Sb1–S3 bond (Fig. 6). The Sb1 cation has two strong bonds to sulfur inside its cluster (2.488 Å to S2 and 2.496 to S5), whereas the third short bond to S1 is stretched, 2.611 Å, and is opposed by the shortest weaker interaction of 2.921 Å to the next cluster. The remaining long interactions of the Sb1 cluster measure 3.262 Å and 3.701 Å; they are oriented to S12 in different 'molecules'. In the (*pseudo*)mirror-symmetrical position Sb4, the analogous short bond is Sb4–S12, and it is 2.430 Å long.

Outer surfaces of the approximately square-shaped clusters are full of outward-radiating lone electron pairs of Sb and/or As. The strong-bond connection takes place only at their corners, *via* As4–S7/S6–As5 connections, bent *via* the covalent As4–S7/S6 and S7/S6–As5 bonds (Figs. 8, 9). Always, two opposing corners of the cluster have trigonal pyramids of As5 with two arms pointing into the meeting space of four columns. They are joined by two As4 atoms *via* common S6/S7 sites. The As4 sites are stabilized by the As3–As4 bonds. All four As atoms in the elongate hexagon-shaped As4–As5–As4–As5 group have lone electron pairs approximately oriented in the same direction. Because of the internal glide plane in each column, this connection occurs in one column only in every second cluster and the contacts of intervening clusters occur *via* weak contacts of As1 polyhedra (Fig. 8). This situation involving both high-force and weak interactions may lead to high-frequency vibrations, and to displacements that contribute to the low-energy vibrations documented by Raman spectroscopy.

DISCUSSION

Related structures

With its pseudo-tetragonal character (Fig. 9) and low content of thallium, the crystal structure of gungerite is unique among Tl–As sulfosalts. Interesting analogies on a more local scale were found between gungerite and gillulyite, $Tl_2(As,Sb)_8S_{13}$ (Foit et al. 1995, revised by Makovicky and Balić-Žunić 1999). The latter structure has the *b* parameter equal to 5.679 Å, *i.e.* one half of the *b* parameter of gungerite**.** It can be interpreted as broad double-ribbons of tightly-bonded SnS-like layers, stacked and separated by lone electron pairs micelles (spaces). Some arsenic polyhedra complicate this scheme, being oriented diagonally to the orientation of the majority of polyhedra. This somewhat reminds of clusters and their spacing in gungerite along the Tl rods.

As one can see in the projection along the *b* axis (Fig. 9), the structure of gillulyite consists of periodically constricted (001) layers separated by spaces with lone electron pairs and long weak interactions. The periodically constricted layer can be understood as stacking of diagonally oriented ellipsoidal arrangements of eight cation sites (occupied by (As, Sb), only the apical ones with Tl–and–(As,Sb) alternation) (Fig. 10). Short cation–sulfur bonds are oriented inwards, and the mostly weak long cation–sulfur distances outwards. This was the pattern recognized also in the Patterson map of gungerite, in which the apices of the ellipses are occupied by thallium, and the six remaining cation sites alternatively by As and Sb (Fig. 10). The corresponding pattern of short bonds and S positions in gungerite partly (but not fully) resembles that seen in gillulyite. The principal difference is that in gillulyite this ellipsoidal configuration is centered above split Tl positions whereas in our case there are Sb/As atoms below it, close to the *foci* of the projected ellipse. It was recognized that they form part of another complete ellipse below the first one, oriented at ~90° to the first one (Fig. 11).

In gungerite, every thallium site forms a part of the [101] string of such ellipsoidal configurations, which have the same overall *y* parameter (Fig. 11). This string runs diagonally

374 to the unit cell axes, as does another string, at 90° to the first one, and with a different *y*
375 parameter. Parallel strings alternatively assume two *y* levels, ½ *b* apart. Another such system
376 of strings runs parallel to the other diagonal. In its totality, this remarkable system of
377 superimposed ellipsoidal arrangements appears to make maximum space for the lone electron
378 pair configurations of As and Sb, especially in the channels which are created by overlapping
379 ellipses (Fig. 11).

380 The other thallium-arsenic sulfosalt which has a columnar structure is lorándite,
381 $TlAsS_2$ (Zemann and Zemann 1979; Fleet 1973; Balić-Žunić et al. 1995). It is situated
382 practically at the opposite pole of the Tl:(As,Sb) spectrum of compositions. In this monoclinic
383 structure, rods are much thinner, each formed by a spiral of As–S coordinations, with the As
384 atoms on the edges of square-shaped rods and with the long interactions (3.953 Å and longer)
385 interconnecting the rods. Tl atoms alternate with the As atoms along the rod edges and Tl–S
386 distances participate in the *rod-to-rod* bonding, unlike those in gungerite.
387
388 *Twinning*
389 As mentioned above, twinning is present in the investigated crystal, with the twinning
390 matrix (0 0 –1/0 1 0 /1 0 0) and the two twin fractions 0.8354(9)/0.1646(9). The simplest
391 twinning model assumes the [010] rods intact, with their internally active *b* glide plane and
392 the chessboard scheme of alternating [010] and [0–10] orientations preserved. One of the
393 (001) rod walls is broader and slightly convex, and it faces the opposite (001) wall of the next
394 rod, which is narrower and slightly concave. As a consequence, the (100) walls are slightly
395 convergent (Fig. 11) and they meet with the like walls of adjacent rods along *a* direction. The
396 rods are interconnected by strong bonds only rarely, in places where four of them meet (Figs.
397 7, 11); all other interspaces between the rods are filled by lone electron pairs and van der
398 Waals contacts.

399 The observed twinning can tentatively be connected with the As–Sb interchange,
400 detected in the majority of cation positions (specified above). Except for Sb1, which
401 interconnects adjacent doughnuts in a rod (unlike its counterpart, Sb4, which is without such
402 interconnection), the pure, unmixed cation sites are situated on rod corners, and not in its
403 walls. Interchange of cations in the latter, wall positions, where they have long-range
404 interactions with opposing rods, might favour the changes connected with twinning. The
405 approximate equality between the volume ratios of twin domains and those of cation ratios in
406 the (As,Sb)1, (As,Sb)2, (Sb,As)2, and (Sb,As)3 positions is strongly suggestive of such
407 connection.

408 On the structure level, twinning is represented by a two-fold screw axis parallel to
409 [101] with a shift of the only ¼ of the full [101] repetition period (Dornberger-Schiff
410 designation $2_{1/2}$; Dornberger-Schiff 1966) instead of ½ of the repetition period (designation
411 2_1) of the usual screw axis. As a result, the given twinning operation is an *OD* (order-disorder)
412 operation and two positions of the twinned domain are possible, either produced by the $2_{1/2}$
413 operation or by $2_{-1/2}$. They become identical on the macrocrystal scale.

414 We were warned that the twin law on the macrocrystal level, (0 0 –1/0 1 0 /1 0 0), also
415 is a matrix for a four-fold twin law with the rotation axis parallel to [010]. Close inspection of
416 the twinned structure, however, shows that the crystal structure orientation after two partial
417 90° rotations is identical to the initial one, except for a small shift of the $a/2+c/2$ size, which is
418 invisible on a macrocrystal. It means that the twin consists of two and not four individuals
419 (crystal orientations) and the twin law is a dichroic four-fold inversion axis, –4, without
420 additional two-fold axes perpendicular to it. It also should be mentioned that there are two
421 categories of twin operation descriptions, one classical, on a macrocrystal level, and another,
422 perhaps non-classical, but describing exactly what happens during twinning on the
423 composition plane; both are given here.

IMPLICATIONS

The crystal structure of gungerite appears to be unique among the structures of Tl–As–Sb sulfides. As a remarkable case of inorganic structural architecture, '*doughnuts*' which display imperfect *reflection* symmetry are in the gungerite structure organized into semi-independent *polar* rods with a glide-plane symmetry; these, in turn, are arranged in a chess-board pattern of [010] and [0–10] rods *via* two additional systems of glide planes, two-fold axes and inversion centers of the *Pbcn* group. The profusion of van der Waals interactions and the presence of sparse covalent interconnections at critical points of the structure make it an interesting object of future structural dynamics studies.

ACKNOWLEDGMENTS

Three anonymous reviewers and Associate Editor Diego Gatta are thanked for constructive comments, which improved the manuscript. The friendly interest of Dr. T. Balić-Žunić and further colleagues involved in the studies of arsenic-rich Tl mineralizations is acknowledged with pleasure. We acknowledge CzechNanoLab Research Infrastructure supported by MEYS CR (LM2018110) for the financial support of the measurements. The interpretation of the Raman spectrum was performed in accordance with the state task, state registration No. AAAA-A19-119092390076-7.

REFERENCES

Balić-Žunić, T., Makovicky, E. and Moëlo, Y. (1995) Contributions to the crystal chemistry of thallium sulphosalts. III. The crystal structure of lorandite ($TlAsS_2$) and its relation to weissbergite ($TlSbS_2$). Neues Jahrbuch für Mineralogie – Abhandlungen, **168**, 213–235.

448 Bindi, L., Bonazzi, P., Zoppi, M. and Spry, P.G. (2014) Chemical variability in
449 wakabayashilite: a real feature or an analytical artifact? Mineralogical Magazine, **78**, 693–
450 702.
451 Cheng, H., Zhou, Y. and Frost, R.L. (2017) Structure comparison of orpiment and realgar by
452 Raman spectroscopy. Spectroscopy Letters, **50**, 23–29.
453 Dornberger-Schiff, K. (1966) Lehrgang über OD-Strukturen. Akademie-Verlag, Berlin.
454 Fleet, M.E. (1973) The crystal structure and bonding of lorándite, $Tl_2As_2S_4$. Zeitschrift für
455 Kristallographie, **138**, 147–160.
456 Foit, F.F. Jr., Robinson, P.D. and Wilson, J.R. (1995) The crystal structure of gillulyite,
457 $Tl_2(As,Sb)_8S_{13}$ from the Mercur gold deposit, Tooele. County, Utah, U.S.A. American
458 Mineralogist, **80**, 394–399.
459 Forneris, R. (1969) Infrared and Raman spectra of realgar and orpiment. American
460 Mineralogist, **54**, 1062–1074.
461 Frost, R.L., Bahfenne, S. and Keeffe, E.C. (2010) Raman spectroscopic study of the mineral
462 gerstleyite $Na_2(Sb,As)_8S_{13}\cdot 2H_2O$ and comparison with some heavy-metal sulfides.
463 Journal of Raman Spectroscopy, **41**, 1779–1783.
464 Gresham, C. and Lawrey, E. A. (2018). Thallium Toxicity. Medscape;
465 https://emedicine.medscape.com/article/821465-overview.
466 Ikramuddin, M. (1985) Thallium in various types of gold deposits. Conference: 98th annual
467 meeting of the Geological Society of America, Orlando, FL, USA, 28 Oct 1985, Geol.
468 Soc. Am., Abstr. Programs, Vol. 17.
469 Karbowska, B. (2016) Presence of thallium in the environment: sources of contaminations,
470 distribution and monitoring methods. Environmental Monitoring and Assessment, **188**
471 (11), 640.

Kasatkin, A.V., Nestola, F., Agakhanov, A.A., Škoda, R., Karpenko, V.Y., Tsyganko, M.V. and Plášil, J. (2018a) Vorontsovite, $(Hg_5Cu)_{\Sigma 6}TlAs_4S_{12}$, and Ferrovorontsovite, $(Fe_5Cu)_{\Sigma 6}TlAs_4S_{12}$: The Tl- and Tl-Fe-Analogues of Galkhaite from the Vorontsovskoe Gold Deposit, Northern Urals, Russia. Minerals, **8**, 185.

Kasatkin, A.V., Makovicky, E., Plášil, J., Škoda, R., Agakhanov, A.A., Karpenko, V.Y. and Nestola, F. (2018b) Tsygankoite, $Mn_8Tl_8Hg_2(Sb_{21}Pb_2Tl)\Sigma_{24}S_{48}$, a New Sulfosalt from the Vorontsovskoe Gold Deposit, Northern Urals, Russia. Minerals, **8**, 218.

Kasatkin, A.V., Makovicky, E., Plášil, J., Škoda, R., Chukanov, N., Stepanov, S., Agakhanov, A.A. and Nestola, F. (2019) Gladkovskyite, $MnTlAs_3S_6$, a new thallium sulfosalt from the Vorontsovskoe gold deposit, Northern Urals, Russia. Journal of Geosciences, **64**, 207–218.

Kasatkin, A.V., Makovicky E., Plášil, J., Škoda, R., Agakhanov, A.A., Stepanov, S.Y. and Palamarchuk, R.S. (2020a) Luboržákite, Mn_2AsSbS_5, a new member of pavonite homologous series from Vorontsovskoe gold deposit, Northern Urals, Russia. Mineralogical Magazine, **84**, 738–745.

Kasatkin A.V., Makovicky E., Plášil J., Škoda R., Agakhanov A.A., Tsyganko M.V. (2020b) Pokhodyashinite, IMA 2019–130. CNMNC Newsletter No. 55; Mineralogical Magazine, **84**, 485–488.

Kasatkin, A.V., Stepanov, S.Yu., Tsyganko, M.V., Škoda, R., Nestola, F., Plášil, J., Makovicky, E., Agakhanov, A.A., Palamarchuk, R.S. (2020c) Mineralogy of the Vorontsovskoe gold deposit (Northern Urals). Part 1: History of study, mineral assemblages, list of minerals. Mineralogiya, **6**(4), 3–34 (in Russian).

Kasatkin A.V., Plášil J., Makovicky E., Chukanov N.V., Škoda R., Agakhanov A.A., Stepanov S.Y. and Palamarchuk R.S. (2021) Auerbakhite, $MnTl_2As_2S_5$, a new thallium

sulfosalt from the Vorontsovskoe gold deposit, Northern Urals, Russia. Journal of Geosciences, **66**(2), DOI: 10.3190/jgeosci.321.

Kharbish, S. (2011) Raman spectroscopic investigations of some Tl-sulfosalt minerals containing pyramidal $(As,Sb)S_3$ groups. American Mineralogist, **96**, 609–616.

Kharbish, S., Libowitzky, E. and Beran, A. (2009) Raman spectra of isolated and interconnected pyramidal XS_3 groups (X = Sb, Bi) in stibnite, bismuthinite, kermesite, stephanite and bournonite. European Journal of Mineralogy, **21**, 325–333.

Kraus, W. and Nolze, G. (1996) POWDER CELL - a program for the representation and manipulation of crystal structures and calculation of the resulting X-ray powder patterns. Journal of Applied Crystallography, **29**, 301–303.

Laugier, J. and Bochu, B. (2003) CELREF: Unit-Cell Refinement Program from Powder Diffraction Diagram. Laboratoires des Matériaux et du Génie Physique, Ecole Nationale Supérieure de Physique de Grenoble (INPG), Grenoble, France.

Makovicky, E. (2006) Crystal structures of sulfides and other chalcogenides. Reviews in Mineralogy and Geochemistry, **61**, 7–125.

Makovicky, E. (2018) Modular crystal chemistry of thallium sulfosalts. Minerals, **8**, 478.

Makovicky, E. and Balić-Žunić, T. (1998) Contribution to the crystal chemistry of thallium sulfosalts. IV. Modular description of Tl–As–Sb sulfosalts rebulite and jankovićite. Neues Jahrbuch für Mineralogie – Abhandlungen, **174**, 181–210.

Makovicky, E. and Balić-Žunić, T. (1999) Gillulyite $Tl_2(As,Sb)_8S_{13}$: Reinterpretation of the crystal structure and order-disorder phenomena. American Mineralogist, **84**, 400–406.

Makreski, P., Jovanovski, G. and Boev, B. (2014) Micro-Raman spectra of extremely rare and endemic Tl-sulfosalts from Allchar deposit. Journal of Raman Spectroscopy, **45**, 610–617.

Mernagh, T.P. and Trudu, A.G. (1993) A laser Raman microprobe study of some geologically important sulphide minerals. Chemical Geology, **103**, 113–127.

Minceva-Sukarova, B., Jovanovski, G., Makreski, P., Soptrajanov, B., Griffith, W., Willis, R. and Grzetic, I. (2003) Vibrational spectra of $M^{I}M^{III}S_2$ type synthetic minerals (M^{I} = Tl or Ag and M^{III} = As or Sb). Journal of Molecular Structure, **651-653**, 181–189.

Morimoto, N. (1954) The crystal structure of orpiment (As_2S_3) refined. Mineralogical Journal, **1**, 160–169.

Mullen, D.J.E. and Nowacki, W. (1972) Refinement of the crystal structures of realgar, AsS and orpiment, As_2S_3. Zeitschrift für Kristallographie, **136**, 48–65.

Muniz-Miranda, M., Sbrana, G., Bonazzi, P., Menchetti, S. and Pratesi, G. (1996) Spectroscopic investigation and normal mode analysis of As_4S_4 polymorphs. Spectrochimica Acta A, **52**, 1391–1401.

Murzin V.V., Naumov E.A., Azovskova O.B., Varlamov D.A., Rovnushkin M.Yu. and Pirajno F. (2017) The Vorontsovskoe Au-Hg-As ore deposit (Northern Urals, Russia): Geological setting, ore mineralogy, geochemistry, geochronology and genetic model. Ore geology reviews, **85**, 271–298.

Petříček, V., Dušek, M. and Palatinus, L. (2014) Crystallographic computing system Jana2006: general features. Zeitschrift für Kristallographie, **229**, 345–352.

Petříček, V., Dušek, M. and Plášil, J. (2016) Crystallographic computing system Jana2006: Solution and refinement of twinned structures. Zeitschrift für Kristallographie, **231**, 583–599.

Rigaku (2019): CrysAlis CCD and CrysAlis RED. Rigaku-Oxford Diffraction Ltd, Yarnton, Oxfordshire, UK.

Sazonov, V.N., Murzin, V.V. and Grigor'ev, N.A. (1998) Vorontsovsk Gold Deposit: An Example of Carlin-type Mineralization in the Urals, Russia. Geology of ore deposits, **40**, 2, 139–151.

Sheldrick, G.M. (2015) SHELXT – integrated space-group and crystal-structure determination. Acta Crystallographica, **A71**, 3–8.

Thomas, R. and Davidson, P. (2010) Hambergite-rich melt inclusions in morganite crystals from the Muiane pegmatite, Mozambique and some remarks on the paragenesis of hambergite. Mineralogy and Petrology, **100**, 227–239.

Turekian, K.K. and Wedepohl, K.H. (1961) Distribution of the Elements in some major units of the Earth's crust. Geological Society of America, Bulletin, **72**, 175–192.

Vikentyev, I.V., Tyukova E.E., Murzin, V.V., Vikent'eva, O.V. and Pavlov, L.G. (2016) Vorontsovsk gold deposit. Geology, gold modes, genesis. Ekaterinburg: Fort Dialog-Iset, 204 p. (in Russian).

Zemann, A. and Zemann, J. (1979) Zur Kenntnis der Kristallstruktur von Lorandit, $TlAsS_2$. Acta Crystallographica, **12**, 1002–1006.

Captions to figures

Figure 1. Orange fine-grained aggregates of gungerite in carbonate breccia with black powdery greigite. Size of the sample: 5 × 4 cm. Photo: A. D. Kasatkina.

Figure 2. Massive aggregates of gungerite (white) in calcite (medium grey) and quartz (dark grey) matrix. Polished section, SEM (BSE) image.

Figure 3. The Raman spectrum of gungerite (excited by 633 nm laser). The experimental spectrum is displayed as a solid black line. The black dotted curve which matches the black line is a result of a spectral fit as a sum of individual Voigt peaks (orange) shown below the curve.

Figure 4 Pseudotetragonal single-crystal X-ray diffraction pattern of gungerite. **a)** Simulated *h*1*l* layer of the reciprocal space of gungerite. Reflections from the two domains overlap completely (except of the few reflections on the zero rows) due to twinning by metric merohedry. Two twin domains of the gungerite unit-cell are displayed as red and green squares. **b)** Reciprocal space reconstruction (*UNWARP* tool) of the *h*1*l* layer from the experimental X-ray data. Simulation done from the refinement reflection file in Jana2006. The radii of the reflections are scaled by their intensities.

Figure 5. Chelating As/Sb group, inserted thallium atom and an As5 'plug' from another group, form together a unit-cluster of the gungerite structure. In all figures, large yellow spheres are S, large blue spheres Tl, red spheres (grey strong bonds) are Sb, and brown spheres (brown strong bonds) are As. Covalent As–As bonds displayed in mauve.

Figure 6. Four clusters ('*doughnuts'*) formed by concatenated As- and Sb-coordination pyramids, strung along a rod of coordination polyhedra of thallium (in azure).

Figure 7. Two chains consisting of thallium (blue) with the attached clusters formed by As- and Sb-pyramids. Correlation between cluster orientations results in column interconnections as illustrated.

Figure 8. Interconnection of four adjacent *rod-and-cluster* columns across the interspace. The drawing contains corner configurations from four columns and the corresponding bridging atoms and bonds. Thin lines (in gold) describe long cation–anion interactions.

Figure 9. Crystal structure of gungerite projected along [010]. In the drawing, the ***a*** axis is horizontal, ***c*** axis is vertical. The space in between the rods is filled with lone-electron pairs of Sb and As.

Figure 10. Elliptical arrangement of As, Sb and apical (Tl, Sb) atoms in one (010) slab of the crystal structure of gillulyite. The inclined ellipses are tightly packed and share some cations. They are underlain by split Tl sites, unlike those in gungerite.

Figure 11. Elliptical arrangement of As, Sb and apical Tl atoms *in one (010) slab* of 'doughnut' clusters in gungerite. Configurations between the intersecting rows of ellipses represent compressed As4–As5–As4–As5 rings and covalently bonded As3–As4 pairs.

601 Alternative diagonal strings of ellipses are positioned halfway between the indicated ones, *on*
602 *the other (010) level of clusters, 0.5 b apart*.
603
604 Figure 12. Visualization of twinning in the crystal structure of gungerite. The composition
605 'plane' is represented here by a *zig-zag* contact *via* long-range interactions instead of a
606 hypothetical 'planar' contact. The [010] and [0–10] oriented rods are distinguished by
607 coloring, forming a chessboard pattern in both domains. Axis orientation is indicated for both
608 domains.
609

610

611 Table 1. Reflectance values of gungerite (in %)

λ (nm)	R_1	R_2	λ (nm)	R_1	R_2
400	33.3	27.8	560	27.0	25.7
420	31.1	27.7	580	26.2	25.1
440	30.1	26.5	**589**	**25.9**	**24.5**
460	29.8	26.7	600	25.6	24.0
470	**29.8**	**27.0**	620	24.9	23.5
480	29.9	27.3	640	24.2	22.8
500	29.4	27.4	**650**	**23.9**	**22.4**
520	28.5	26.8	660	23.5	21.9
540	27.6	26.3	680	22.9	21.0
546	**27.4**	**26.1**	700	22.4	20.4

612 The four wavelengths required by the COM of the IMA are given in bold characters.

613

614 Table 2. Chemical composition of gungerite based on electron microprobe data

615

Constituent	wt%	Range	SD	Probe Standard
Tl	13.68	13.37–14.13	0.22	Tl(Br,I)
As	26.77	25.32–27.49	0.71	pararammelsbergite
Sb	30.97	30.45–31.40	0.24	Sb
S	28.02	27.21–28.98	0.60	chalcopyrite
Total	99.44			

616

617

618 Table 3. Powder X-ray diffraction data for gungerite (the d_{hkl} spacings are given in Å).

$I_{rel.}$ (%)	d_{obs}	d_{calc}	I_{calc}	h	k	l
1	10.047	10.083	23	2	0	0
3	8.957	8.985	22	1	1	1
1	7.153	7.122	3	2	0	2
100	5.755	5.759	68	0	2	0
1	5.593	5.578	20	3	1	1
1	5.337	5.339	8	1	2	1
1	5.026	5.041	8	4	0	0
1	4.844	4.851	<1	1	2	2
2	4.479	4.478	60	2	2	2
4	4.273	4.274	28	3	2	1
		4.270	24	1	2	3
6	3.705	3.707	37	1	3	1
1	3.661	3.663	100	3	2	3
1	3.564	3.549	18	4	2	2
		3.546	21	2	2	4
2	3.379	3.380	32	2	3	2
1	3.342	3.366	50	6	0	0
		3.353	48	0	0	6
1	3.311	3.310	10	5	1	3
1	3.329	3.289	6	3	3	1
1	3.070	3.072	31	6	1	2
10	3.030	3.029	23	4	2	4
10	2.901	2.903	27	6	2	0
14	2.878	2.880	15	0	4	0
5	2.850	2.851	3	0	4	1
10	2.821	2.822	42	1	4	1
1	2.769	2.768	3	0	4	2
		2.763	20	1	1	7
1	2.670	2.670	22	2	4	2
1	2.624	2.624	3	1	4	3
1	2.557	2.556	27	7	2	1
1	2.504	2.500	5	7	0	4
1	2.289	2.286	14	1	3	7
2	2.274	2.274	12	1	5	1
1	2.248	2.247	9	2	2	8
1	2.236	2.239	2	4	4	4
		2.232	1	2	5	1
1	2.212	2.211	7	3	4	5
1	2.191	2.195	15	6	2	6
1	2.128	2.124	1	5	4	4
1	2.092	2.096	2	8	3	1
1	1.780	1.780	17	8	0	8
1	1.727	1.727	11	5	6	1
1	1.425	1.424	3	10	0	10

619

620

This is the peer-reviewed, final accepted version for American Mineralogist, published by the Mineralogical Society of America.
The published version is subject to change. Cite as Authors (Year) Title. American Mineralogist, in press.
DOI: https://doi.org/10.2138/am-2022-8003. http://www.minsocam.org/

Table 4. Data collection and structure refinement details for gungerite.

Diffractometer	SuperNova Rigaku micro-diffractometer
X-ray radiation	Mo$K\alpha$ (λ = 0.71075 Å)
Temperature	286 K
Chemical formula	$TlAs_{5.293}Sb_{3.707}S_{13}$
Space group	*Pbcn*
Unit cell dimensions	a = 20.1958(3) Å
	b = 11.5258(2) Å
	c = 20.1430(2) Å
V	4688.74(12) Å^3
Z	8
$\rho_{calc.}$ (for above formula)	4.162 g·cm^{-3}
Absorption coefficient	19.633 mm^{-1}
F(000)	5222
Crystal size	0.28 × 0.18 × 0.11 mm
θ range	4.53 to 27.75°
Index ranges	$-26 \le h \le 26$, $-14 \le k \le 14$, $-26 \le l \le 26$
Reflections collected/unique	114573/5652; R_{int} = 0.0716
Reflections with $I > 3\sigma I$	4790
Completeness to θ = 27.75°	97%
Refinement method	Full-matrix least-squares on F^2
Parameters/restraints	214/0
GoF	1.82
Final R indices [$I > 3\sigma(I)$]	R_1 = 0.0373, wR_2 = 0.1213
R indices (all data)	R_1 = 0.0501, wR_2 = 0.1266
Weighting scheme, weights	Weighting scheme based on measured s.u.'s; $w = 1/(\sigma^2(I) + 0.0025I^2)$
Largest diff. peak/hole	+1.38/–1.31 e·Å^{-3}
Twin matrix; Tw_{vol1}/Tw_{vol2}	$\begin{pmatrix} 0 & 0 & -1 \\ 0 & 1 & 0 \\ 1 & 0 & 0 \end{pmatrix}$; 0.8354(9)/0.1646(9)

This is the peer-reviewed, final accepted version for American Mineralogist, published by the Mineralogical Society of America.
The published version is subject to change. Cite as Authors (Year) Title. American Mineralogist, in press.
DOI: https://doi.org/10.2138/am-2022-8003. http://www.minsocam.org/

Table 5. Atom coordinates, equivalent displacement parameters (in $Å^2$) and occupational factors (Occ.) for gungerite.

Atom	*x/a*	*y/b*	*z/c*	U_{eq}	*Occ.*
Tl1	0.24226(3)	0.20605(5)	0.50810(3)	0.03918(18)	
Sb1	0.39295(4)	0.12605(7)	0.66069(4)	0.0250(2)	
Sb2/Sb2’	0.07501(4)	0.40811(8)	0.45577(5)	0.0283(3)	0.840(12)Sb/0.160(12)As
Sb3/Sb3’	0.29719(4)	0.38533(7)	0.68080(4)	0.0276(3)	0.844(13)Sb/0.156(13)As
Sb4/Sb4’	0.09147(4)	0.16104(7)	0.35455(4)	0.0257(3)	0.781(11)Sb/0.219(11)As
As1/As1’	0.43140(5)	0.37921(10)	0.55607(5)	0.0247(4)	0.820(12)As/0.180(12)Sb
As2/As2’	0.20330(5)	0.40234(10)	0.32389(6)	0.0226(4)	0.938(12)As/0.062(12)Sb
As3	0.35761(6)	0.30182(9)	0.39780(6)	0.0222(3)	
As4	0.43974(6)	0.25441(10)	0.31259(6)	0.0247(3)	
As5	0.39823(6)	0.21156(10)	0.15027(6)	0.0248(3)	
S1	0.41390(14)	0.3368(3)	0.70323(14)	0.0246(8)	
S2	0.41286(14)	0.1821(3)	0.54310(14)	0.0235(8)	
S3	0.34058(14)	0.0806(2)	0.09520(15)	0.0271(8)	
S4	0.08958(15)	0.2036(3)	0.47605(15)	0.0252(8)	
S5	0.27333(14)	0.1806(3)	0.66270(15)	0.0245(8)	
S6	0.37608(16)	0.1333(3)	0.25265(16)	0.0319(9)	
S7	0.49909(15)	0.1287(3)	0.12794(16)	0.0311(9)	
S8	0.20989(14)	0.2062(2)	0.33975(15)	0.0233(8)	
S9	0.32377(15)	0.4411(3)	0.56535(16)	0.0291(9)	
S10	0.31644(15)	0.4279(3)	0.32216(16)	0.0277(9)	
S11	0.19030(16)	0.4640(3)	0.43110(16)	0.0312(9)	
S12	0.05423(14)	0.3589(2)	0.33641(14)	0.0247(8)	
S13	0.43602(15)	0.4168(3)	0.44297(14)	0.0269(8)	

This is the peer-reviewed, final accepted version for American Mineralogist, published by the Mineralogical Society of America.
The published version is subject to change. Cite as Authors (Year) Title. American Mineralogist, in press.
DOI: https://doi.org/10.2138/am-2022-8003. http://www.minsocam.org/

659 Table 6. Selected interatomic distances (in Å) for gungerite.
660

Tl1–S2	3.528(2)	As1–S2	2.317(4)
Tl1–S3^{i}	3.453(2)	As1–S9	2.295(4)
Tl1–S4	3.150(4)	As1–S13	2.320(2)
Tl1–S5	3.190(2)		
Tl1–S8	3.452(2)	As2–S8	2.287(3)
Tl1–S9	3.373(4)	As2–S10	2.303(2)
Tl1–S9^{iii}	3.526(4)	As2–S11	2.289(4)
Tl1–S11	3.514(4)		
Tl1–S11^{iii}	3.470(4)	As3–S10	2.263(4)
		As3–S13	2.256(4)
Sb1–S1	2.610(3)		
Sb1–S2	2.488(2)	As3–As4	2.4487(17)
Sb1–S3^{ii}	2.921(2)		
Sb1–S5	2.497(2)	As4–S6	2.250(4)
		As4–S7^{xii}	2.250(4)
Sb2–S4	2.411(4)	As4–S10	3.200(3)
Sb2–S11	2.466(4)		
Sb2–S12	2.506(2)	As5–S3	2.206(2)
		As5–S6	2.294(4)
Sb3–S1	2.464(2)	As5–S7	2.295(4)
Sb3–S5	2.436(3)		
Sb3–S9	2.473(4)		
Sb4–S4	2.497(2)		
Sb4–S8	2.466(2)		
Sb4–S12	2.429(2)		

661 Symmetry codes: (i) $-x+1/2, -y+1/2, z+1/2$; (ii) $x, -y, z+1/2$; (iii) $-x+1/2, y-1/2, z$; (xii) $-x+1, y, -z+1/2$.
662

This is the peer-reviewed, final accepted version for American Mineralogist, published by the Mineralogical Society of America.
The published version is subject to change. Cite as Authors (Year) Title. American Mineralogist, in press.
DOI: https://doi.org/10.2138/am-2022-8003. http://www.minsocam.org/

1

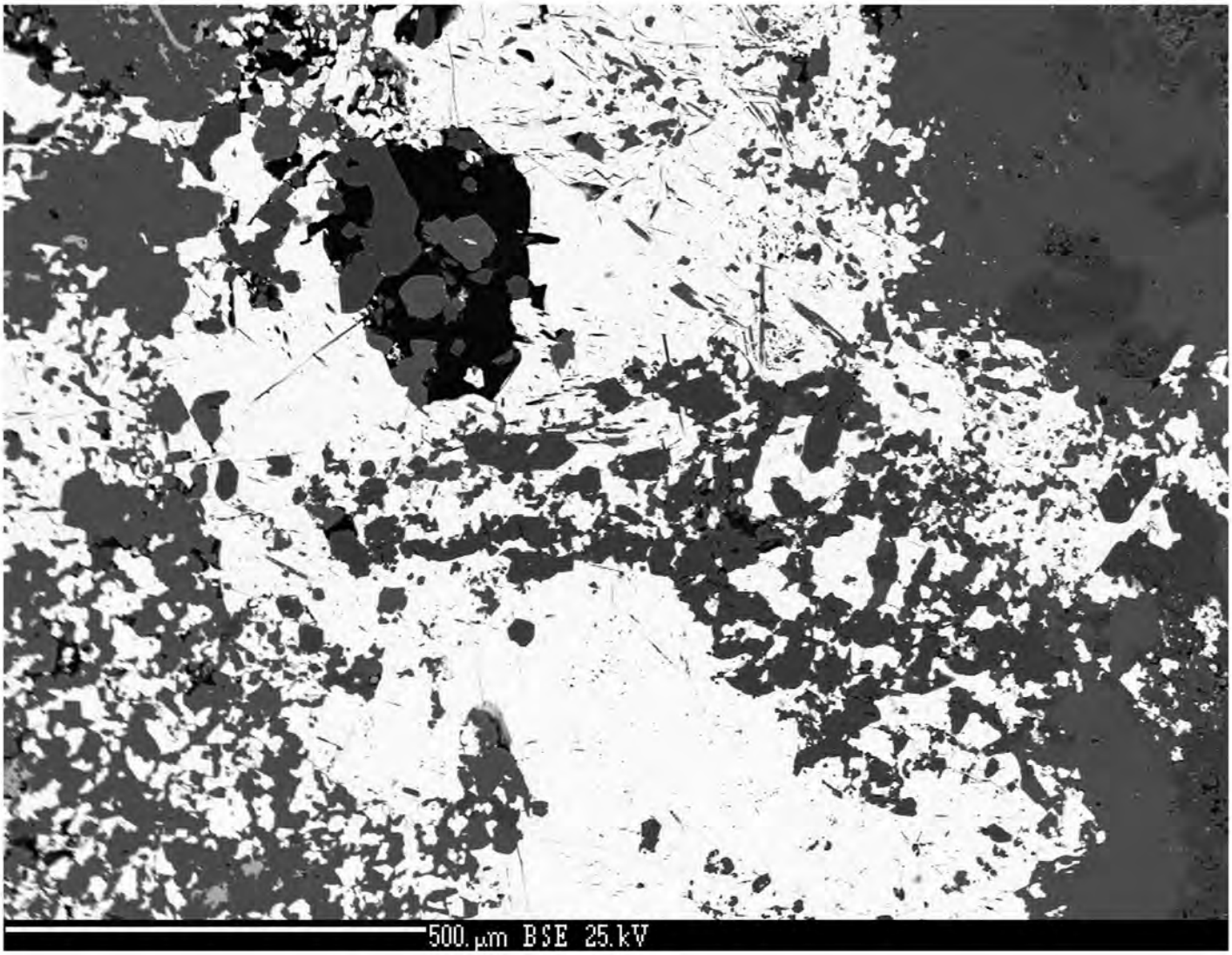

2

This is the peer-reviewed, final accepted version for American Mineralogist, published by the Mineralogical Society of America.
The published version is subject to change. Cite as Authors (Year) Title. American Mineralogist, in press.
DOI: https://doi.org/10.2138/am-2022-8003. http://www.minsocam.org/

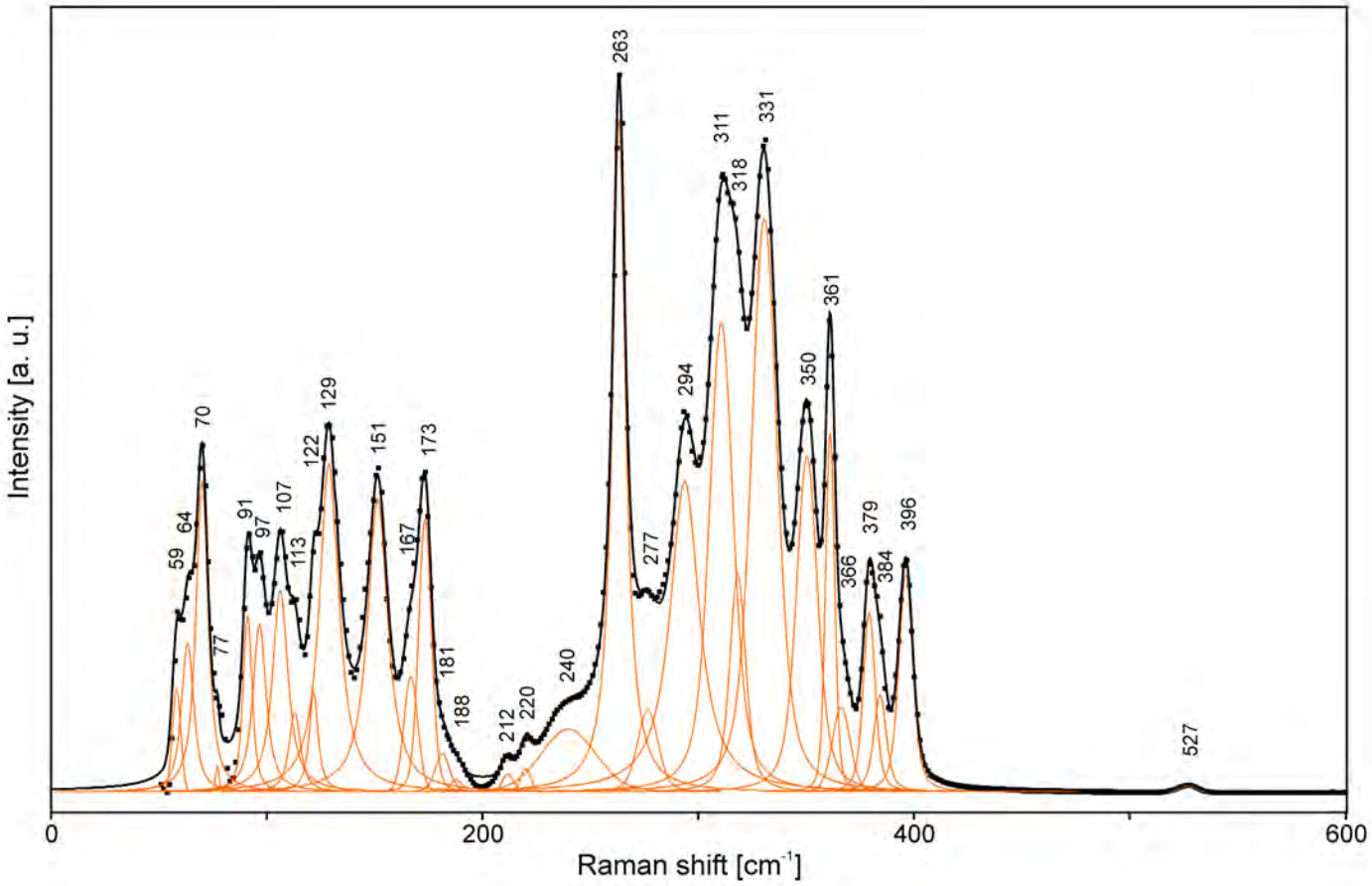

3

This is the peer-reviewed, final accepted version for American Mineralogist, published by the Mineralogical Society of America.
The published version is subject to change. Cite as Authors (Year) Title. American Mineralogist, in press.
DOI: https://doi.org/10.2138/am-2022-8003. http://www.minsocam.org/

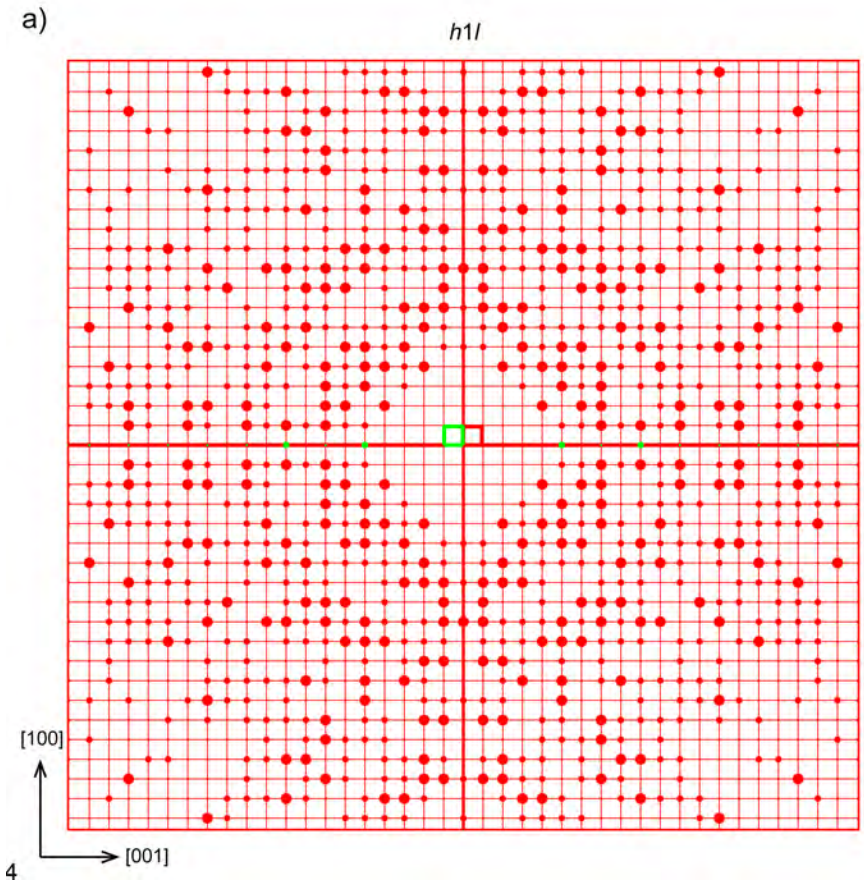

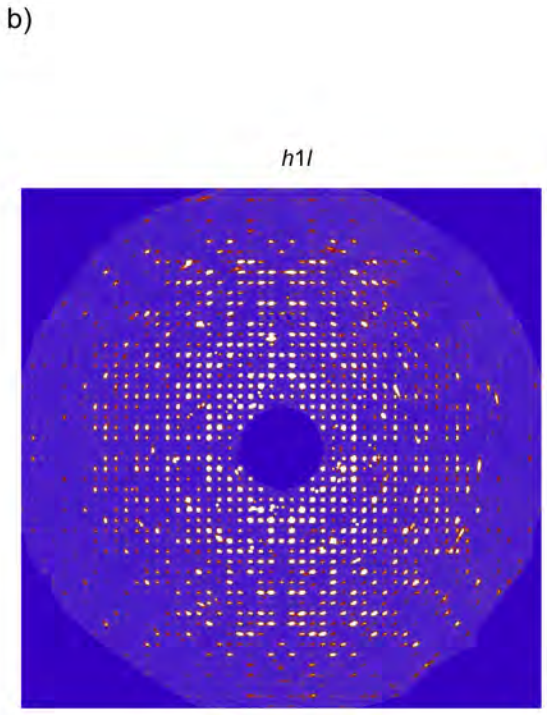

This is the peer-reviewed, final accepted version for American Mineralogist, published by the Mineralogical Society of America.
The published version is subject to change. Cite as Authors (Year) Title. American Mineralogist, in press.
DOI: https://doi.org/10.2138/am-2022-8003. http://www.minsocam.org/

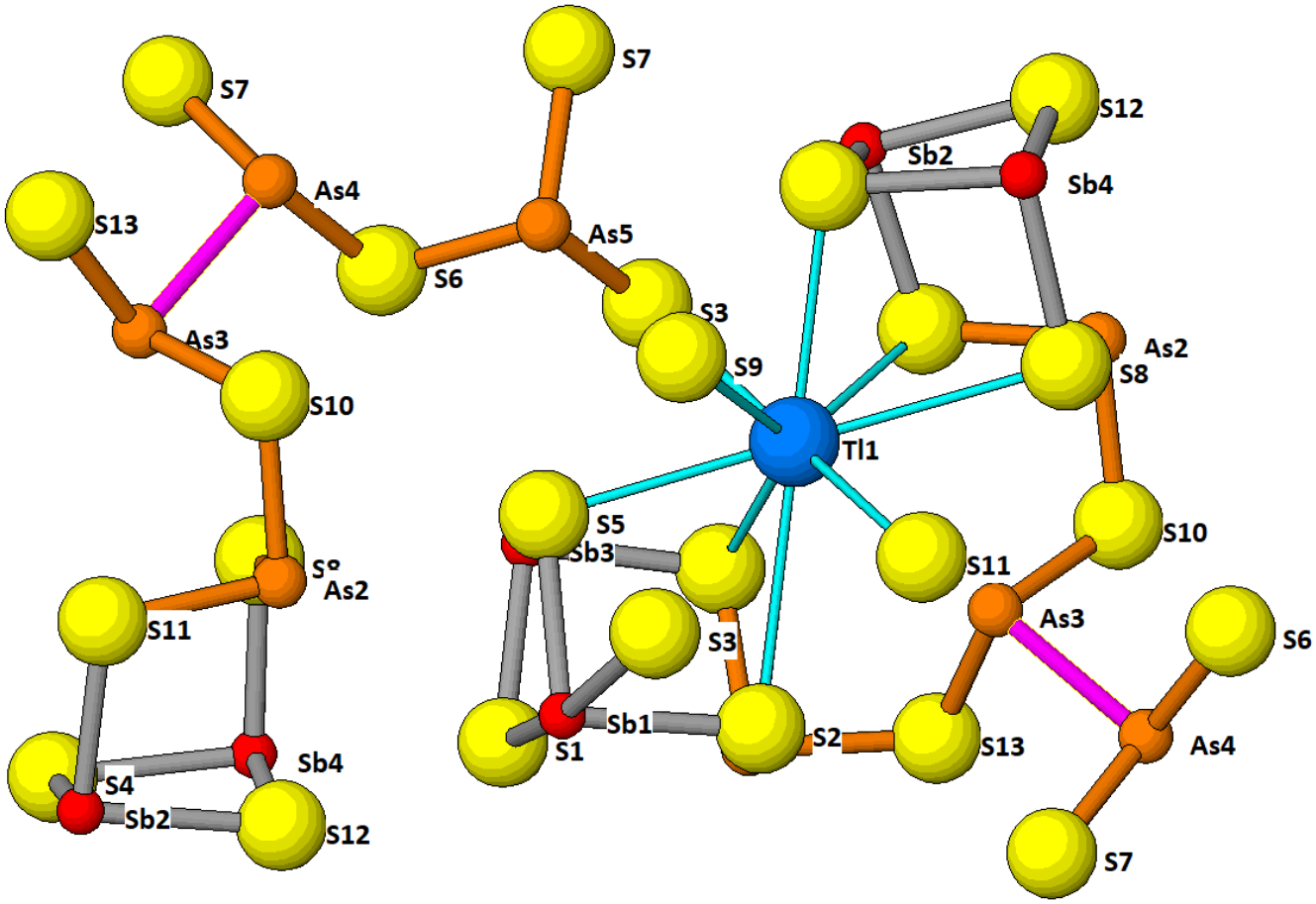

5

This is the peer-reviewed, final accepted version for American Mineralogist, published by the Mineralogical Society of America.
The published version is subject to change. Cite as Authors (Year) Title. American Mineralogist, in press.
DOI: https://doi.org/10.2138/am-2022-8003. http://www.minsocam.org/

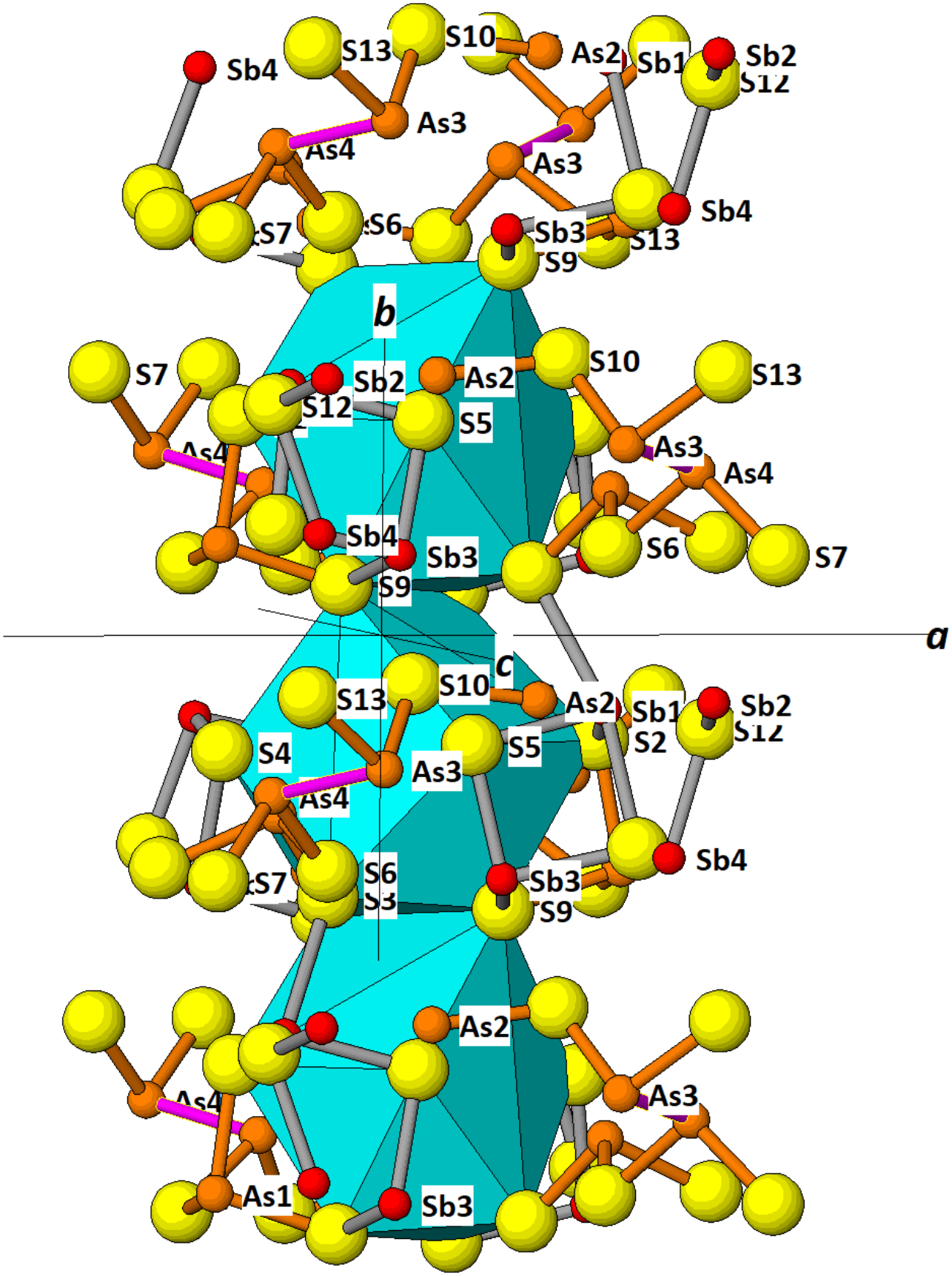

This is the peer-reviewed, final accepted version for American Mineralogist, published by the Mineralogical Society of America.
The published version is subject to change. Cite as Authors (Year) Title. American Mineralogist, in press.
DOI: https://doi.org/10.2138/am-2022-8003. http://www.minsocam.org/

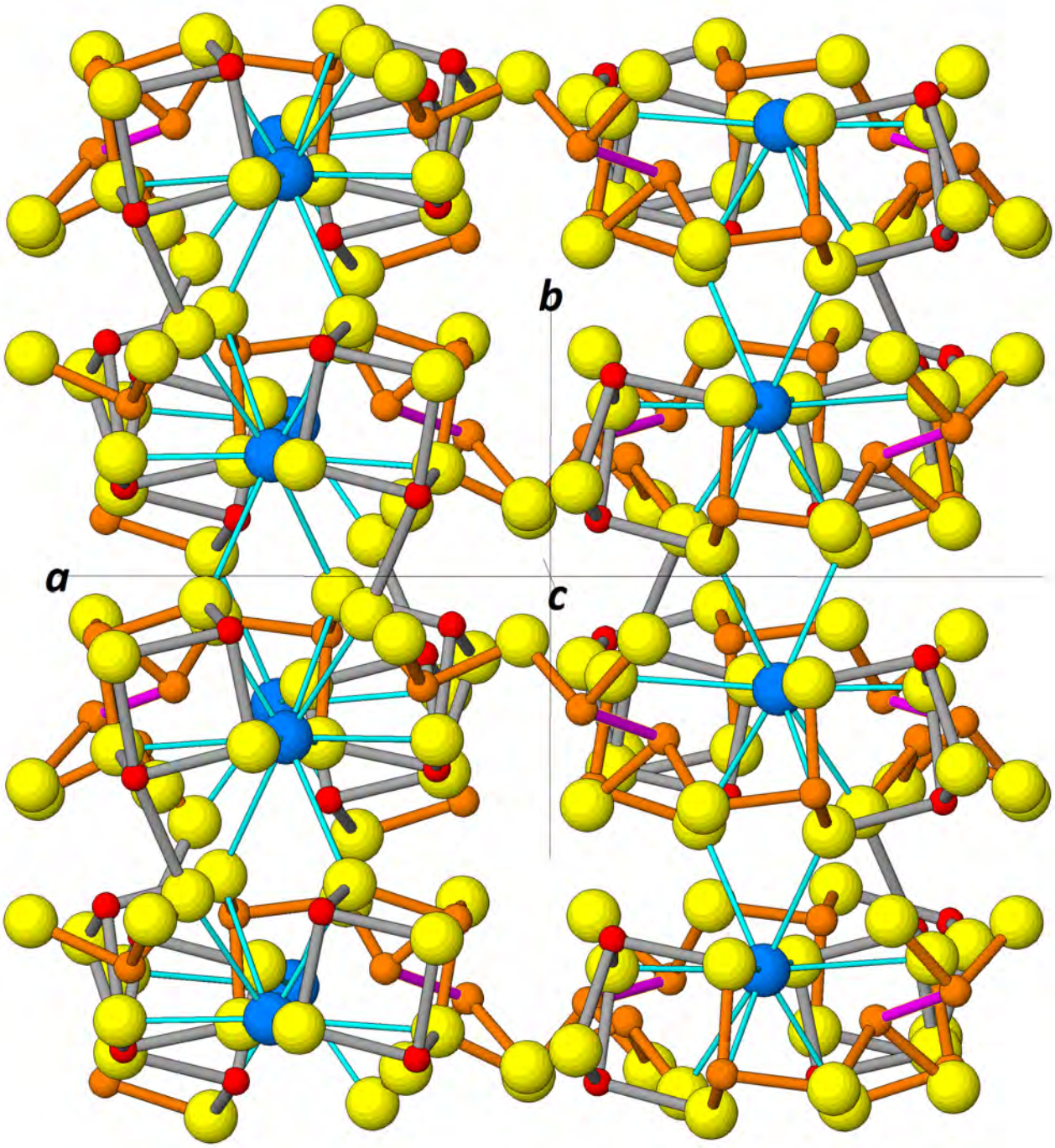

This is the peer-reviewed, final accepted version for American Mineralogist, published by the Mineralogical Society of America.
The published version is subject to change. Cite as Authors (Year) Title. American Mineralogist, in press.
DOI: https://doi.org/10.2138/am-2022-8003. http://www.minsocam.org/

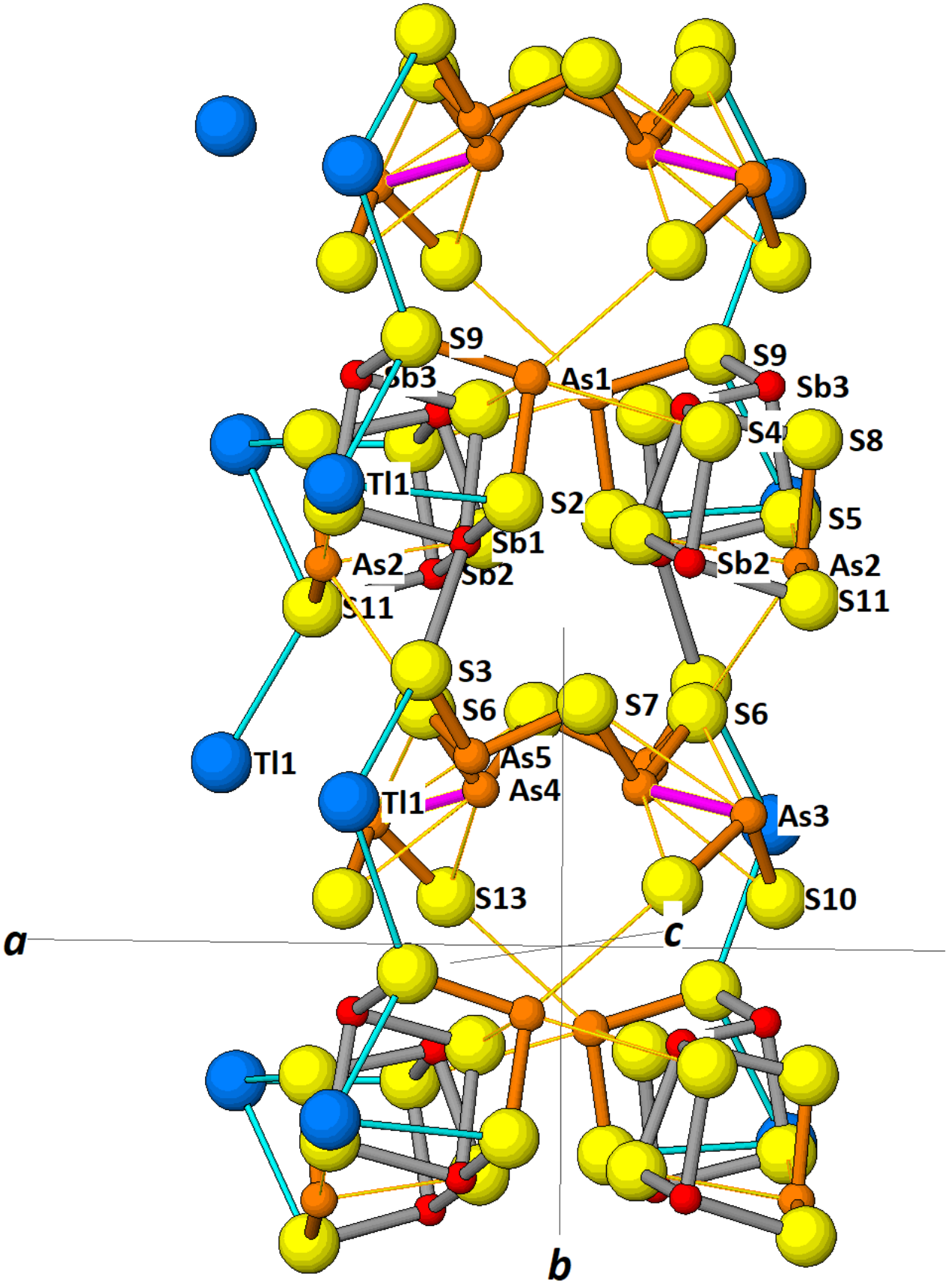

This is the peer-reviewed, final accepted version for American Mineralogist, published by the Mineralogical Society of America.
The published version is subject to change. Cite as Authors (Year) Title. American Mineralogist, in press.
DOI: https://doi.org/10.2138/am-2022-8003. http://www.minsocam.org/

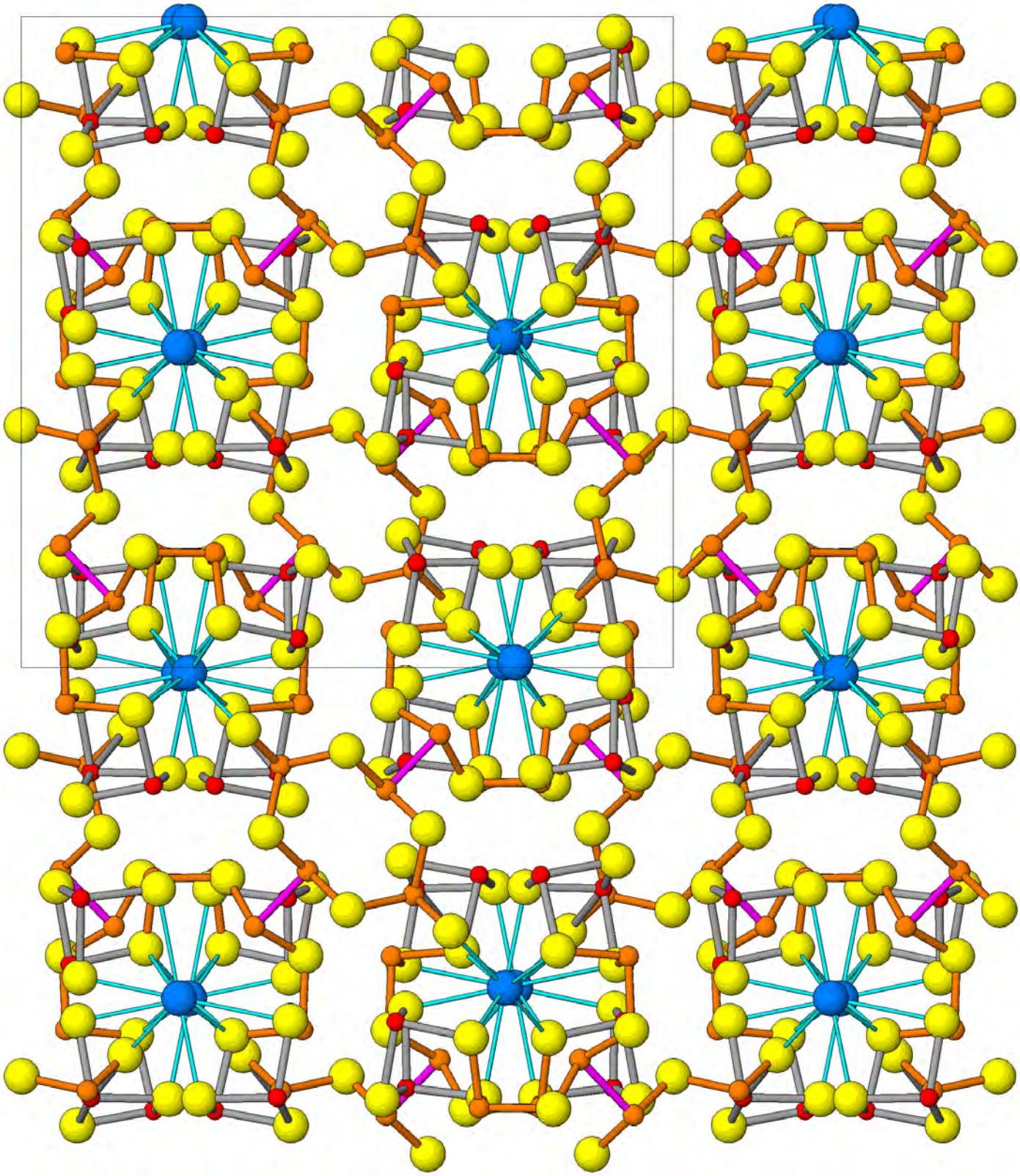

This is the peer-reviewed, final accepted version for American Mineralogist, published by the Mineralogical Society of America.
The published version is subject to change. Cite as Authors (Year) Title. American Mineralogist, in press.
DOI: https://doi.org/10.2138/am-2022-8003. http://www.minsocam.org/

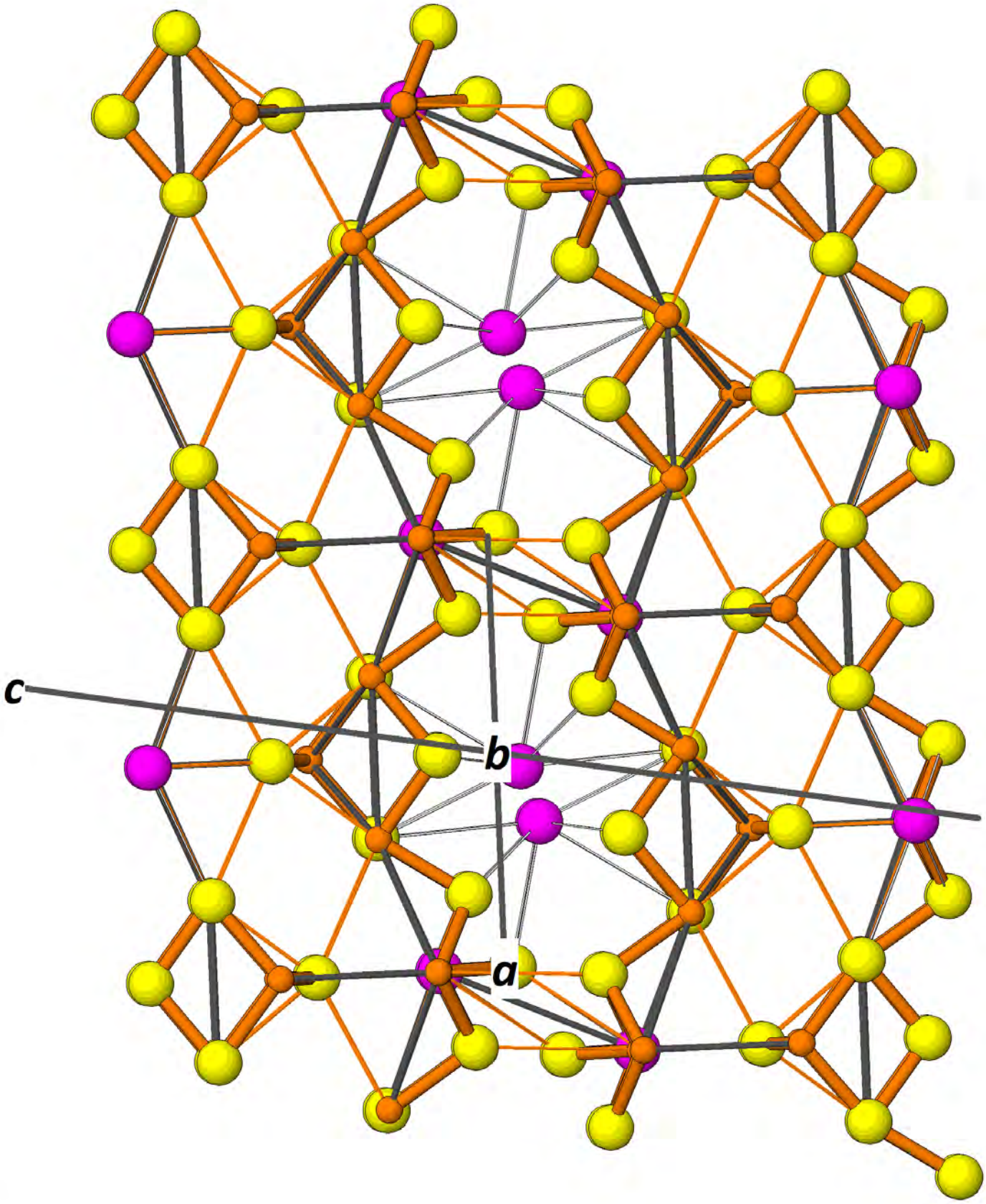

This is the peer-reviewed, final accepted version for American Mineralogist, published by the Mineralogical Society of America.
The published version is subject to change. Cite as Authors (Year) Title. American Mineralogist, in press.
DOI: https://doi.org/10.2138/am-2022-8003. http://www.minsocam.org/

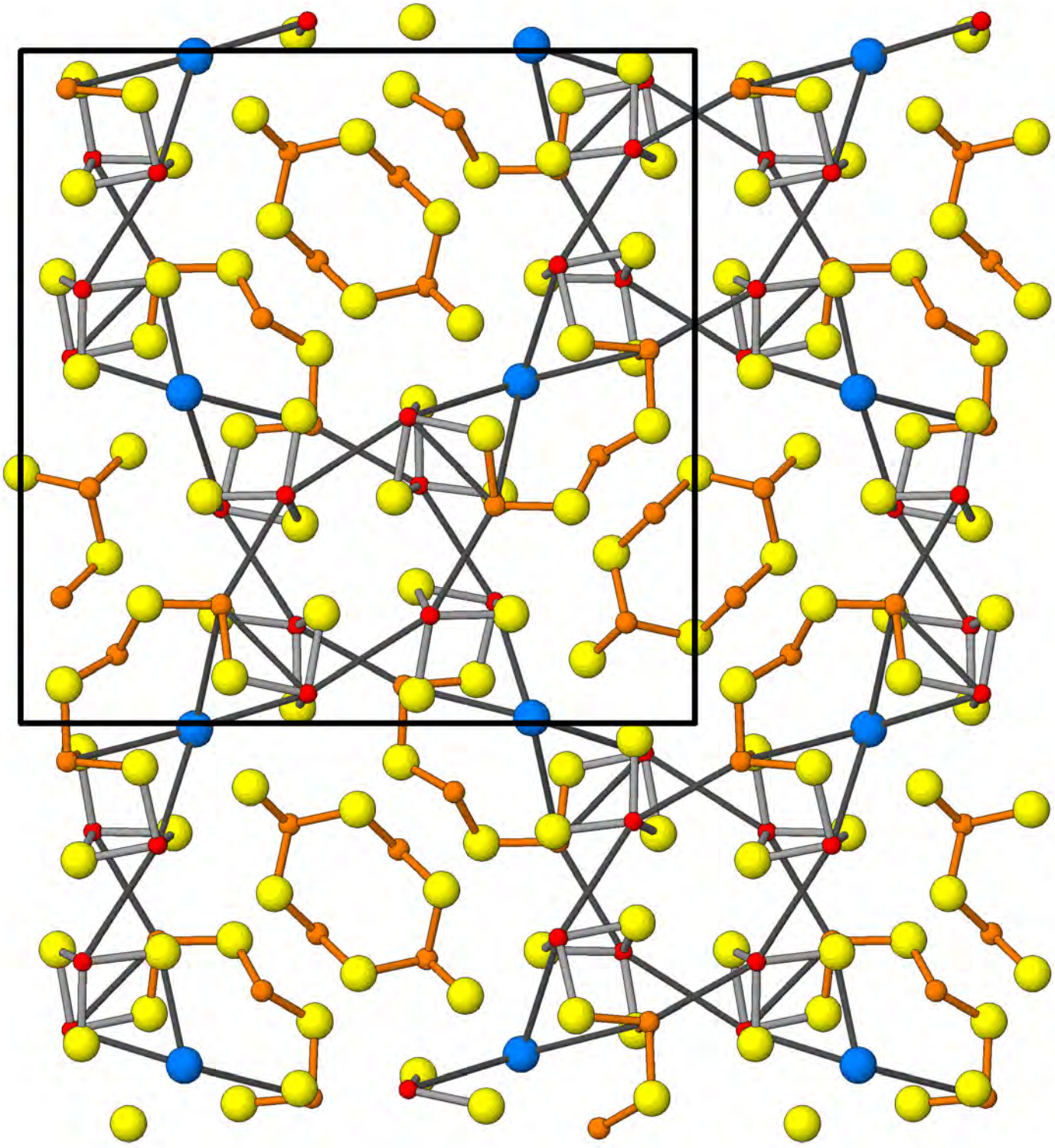

This is the peer-reviewed, final accepted version for American Mineralogist, published by the Mineralogical Society of America.
The published version is subject to change. Cite as Authors (Year) Title. American Mineralogist, in press.
DOI: https://doi.org/10.2138/am-2022-8003. http://www.minsocam.org/